Theoretical study of the structure of boron carbide $B_{13}C_2$

Koun Shirai,* Kyohei Sakuma, and Naoki Uemura
Nanoscience and Nanotechnology Center, The Institute of Scientific and Industrial Research, Osaka University, 8-1 Mihogaoka, Ibaraki, Osaka 567-0047, Japan

(Received 12 March 2014; revised manuscript received 12 August 2014; published 26 August 2014)

We have resolved long-standing discrepancies between the theoretical and experimental crystal structures of boron carbide $B_{13}C_2$. Theoretical studies predict that $B_{13}C_2$ should be stoichiometric and have the highest symmetry of the boron carbides. Experimentally, $B_{13}C_2$ is a semiconductor and many defect states have been reported, particularly in the CBC chain. Reconciling the disordered states of the chain, the chemical composition, and the lowest-energy state is problematic. We have solved this problem by constructing a structural model where approximately three-quarters of the unit cells contain $(B_{11}C)(CBC)$ and one-quarter of them contain $(B_{12})(B_4)$. This structural model explains many experimental results, such as the large thermal factors in x-ray diffraction and the broadening of the Raman spectra, without introducing unstable CBB chains. The model also solves the energy-gap problem. We show that there are many arrangements of these two types of unit cells, which are energetically almost degenerate. This demonstrates that boron carbides are well described by a geometrically frustrated system, similar to that proposed for β-rhombohedral boron.

DOI: 10.1103/PhysRevB.90.064109 PACS number(s): 81.05.Cy, 61.72.Bb, 71.55.Cn

I. INTRODUCTION

Boron carbides have attracted much attention due to their superhardness, thermoelectric properties, and potential use as superconductors [1–5]. Although they are common materials, there are many theoretical difficulties in elucidating their physical and chemical properties.

Boron carbide (B_4C) is a generic name for compounds consisting of B and C, with compositions varying from 20 to 8 at. % or less [6]; B_4C implies a carbon composition of 20%. Although the homogeneity range of boron carbides is a subject of debate [2,7], for theoretical studies, it should be sufficient to regard the representative stoichiometric compounds $B_{12}C_3$ and $B_{13}C_2$ as C rich (20 at. %) and C poor (13.3 at. %), respectively. Boron carbides are semiconductors over the full range of C content.

Boron carbides show a strong propensity for disorder, even though x-ray patterns maintain $R\bar{3}m$ symmetry. $B_{12}C_3$ was initially believed to have a stoichiometric structure, composed of a B_{12} icosahedron plus a three-membered C chain [8]. This structure is symbolically written as $B_{12}(CCC)$. However, later studies showed that a site exchange between the central C atom of the chain and a B atom of the icosahedron takes place (see Fig. 1) [9–12]. This structure is written as $(B_{11}C)(CBC)$. This site exchange has been confirmed by density-functional theory (DFT) calculations, and the preferential site of the icosahedral C atom was determined to be a polar site (p site) [13–15]. A standard view of the structural change from $B_{12}C_3$ to $B_{13}C_2$ is the successive replacement of an icosahedral C atom with a B atom, maintaining the CBC chain, until the stoichiometric compound $B_{12}(CBC)$ is obtained. The $B_{12}(CBC)$ structure has been used in many studies [11,16–19]. However, there is a large discrepancy between theory and experiment. Band calculations predict metallic behavior for $B_{13}C_2$, whereas the compound does not exhibit metallic behavior in experiments. We refer to this discrepancy as the *metal/insulator problem*. This discrepancy is particularly important for the superconducting application [20,21].

Recently, the relationship between stoichiometric defects and electronic properties in boron and boron-rich crystals has been highlighted by experimentalists [22–24]. Table I in Schmechel and Werheit's paper [24] is a useful summary of this relationship. For β-rhombohedral boron, theoretical calculations have demonstrated that the defect states are indeed intrinsic properties [25–29]. This is different from most semiconductors, where defect states are extrinsic properties generated at finite temperatures. Furthermore, theoretical studies have shown that there are many degenerate or almost degenerate defect states in β-rhombohedral boron [27–29], from which Ogitsu *et al.* characterized the structure as a geometrically frustrated system [28,30]. This may be responsible for the insulating properties of β-rhombohedral boron.

Based on these studies, we have examined the general role of the defect states on the insulating properties of boron and boron-rich crystals [31]. For the defect states to fulfill this role, the following conditions must be met. First, an odd number of electrons are required. In band theory, this leads to unfilled bands that result in a metal. However, the second condition is that the crystal must have strong covalency, which alters the behavior of the unfilled bands. The unfilled covalent bonds drive the reconstruction of chemical bonds to fulfill the valence requirement. The third condition is that the unit cell is large enough to have many degrees of freedom for rebonding. The energy barriers for reconstructing unfilled bonds are shared by modest changes of the structure over a large unit cell. Deviation from stoichiometry is a suitable solution for complex crystals to eliminate the unfilled bands.

Presently, the structure of $B_{13}C_2$ is more difficult to investigate than that of β-rhombohedral boron, because both compositional disorder and structural disorder are involved and they are interrelated. Thus, building a coherent picture of the effect of structure on various properties is challenging. The purpose of this study is to apply our mechanism for the insulating properties to $B_{13}C_2$ and to demonstrate that the discrepancies in the defect states and the metal/insulator

*koun@sanken.osaka-u.ac.jp

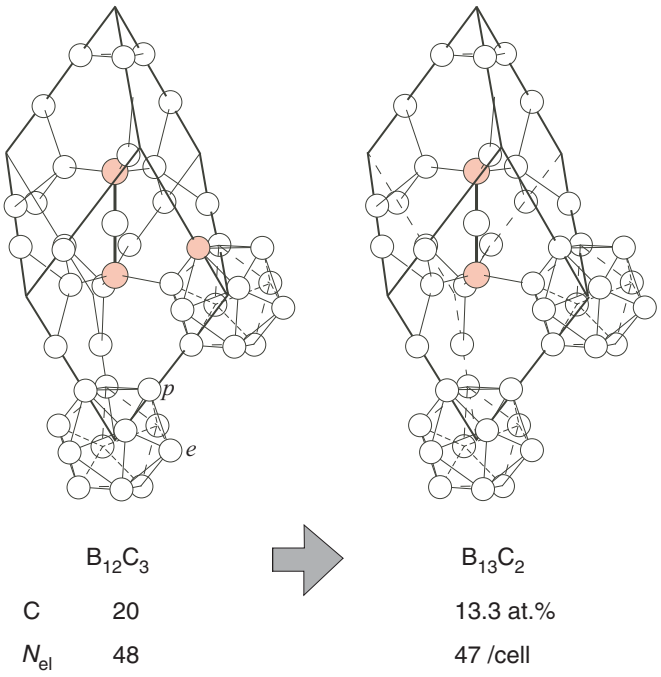

FIG. 1. (Color online) Crystal structure of $B_{12}C_3$ and $B_{13}C_2$. Shaded spheres denote carbon atoms. The p and e sites in the icosahedron are shown.

problem can be resolved. In the next section, we analyze the discrepancies between theoretical and experimental results for $B_{13}C_2$. We identify important features that are required for constructing a crystal model. In Sec. III, we devise an appropriate crystal model for $B_{13}C_2$ based on these features. In Sec. IV, we validate our model by DFT calculations. In Sec. V, we discuss some of the experimental properties of $B_{13}C_2$ in light of our calculations. In the final section, we present a summary of this work.

II. PROBLEMS WITH THE $B_{13}C_2$ STRUCTURE

A. Experimental studies

1. Energy gap

Figure 2 shows a band diagram of $B_{13}C_2$ obtained by local-density approximation (LDA) calculations. An indirect gap of 2.72 eV is seen between the F and L points. Bylander and Kleinman reported a similar value of 2.92 eV [32]. Werheit *et al.* [35] reported an experimental value of 0.48 eV. However, owing to the complicated structure of the energy gap (Fig. 2) [34,36,37], the value was revised to 2.09 eV. Both these calculated values are still larger than the experimental value. Usually, LDA calculations underestimate energy gaps. A tight-band calculation gave a larger value of 3.8 eV for the band gap of $B_{12}C_3$ [38]. Hence, the calculation method is unlikely to account for the discrepancy in energy gaps.

TABLE I. LDA energy differences for the $B_{13}C_2$ structural model reported by Bylander and Kleinman (BK) [32] and our model. The stoichiometric ordered structure B_{12}(CBC) is used as the energy reference. Energy is given in eV/atom.

Model	BK [32]	Present
B_{12}(CBC)	0	0
$(B_{11}C_{(p)})$(CBB)	0.148	0.146
$(B_{11}C_{(e)})$(CBB)	0.140	0.169
$(B_{11}C_{(e')})$(CBB)	0.193	0.121

In the density of states (DOS) of Fig. 2, the Fermi level appears at the top of the valence band, leaving one hole per cell. Therefore, $B_{13}C_2$ should be a metal. This is a result of the odd number of electrons in the unit cell. Experimentally, the electrical conductivity, σ, for all C contents indicates semiconducting behavior. For C-rich $B_{12}C_3$, σ is several $\Omega^{-1}\,\mathrm{cm}^{-1}$ [39–43]. Although σ decreases slightly toward the composition $B_{13}C_2$, there is no evidence that the crystal abruptly changes to a metal at the composition with 13.3 at. % C, as the band calculations predict. It has been suggested that the formation of a Mott insulator could explain this [32]. However, the local moments are small [44]. Thus, theoretical calculations do not yet explain this discrepancy. Conduction is thought to occur through a hopping mechanism [39,42]. Emin and coworkers proposed a small bipolaron hopping mechanism [1,40,45–49]. This model is still under debate [3,50–52].

2. Experimental detection of defect states

We will briefly review the many experimental studies of defect states in boron carbides. The most reliable method for determining crystal structures is x-ray diffraction. However, the method cannot always distinguish boron and carbon, making the unambiguous determination of boron and carbon locations difficult [12,53]. Therefore, the experimental results are still open to interpretation.

X-ray-diffraction analysis shows that the thermal factor of the chain increases as the C content decreases [12,53,54]. This was interpreted as indicating that the chain structure changes from CBC to something else, such as CBB, suggesting that icosahedral C exists even in $B_{13}C_2$. Other studies support this view [10,11]. Kwei and Morosin performed a systematic neutron powder-diffraction study [55], which identified more complicated defect states, even for $B_{13}C_2$.

There are several NMR studies of the defect states of boron carbides [56–59]. A recent theoretical study showed the presence of the $B_{10}C_2$ unit in $B_{12}C_3$ [15]. Kirkpatrick *et al.* [59] reported that about 10% of the icosahedra in $B_{13}C_2$ have a C atom.

Vibrational spectroscopy can be used to investigate another aspect of the defects [5,36,48,50,53,60–63]. Aselage *et al.* observed a broadening of the narrow bands at 490 and 520 cm^{-1} in the Raman spectra of boron carbides as the C content decreased from 20 at. % and proposed that the ordered state of the CBC chain declines as the C content decreases, suggesting a soft chain [48,53,60,61]. The main problem with this suggestion may be the assignment of these bands, which will be discussed later. Werheit *et al.* obtained Raman spectra by using an excitation laser at a different wavelength and interpreted their data differently [36,50,63]. Although details are different, it is evident that there is a mixture of different chain structures, such as CBC, CBB, and B□B (□ denotes a vacancy). Infrared spectra provide further evidence for this [62].

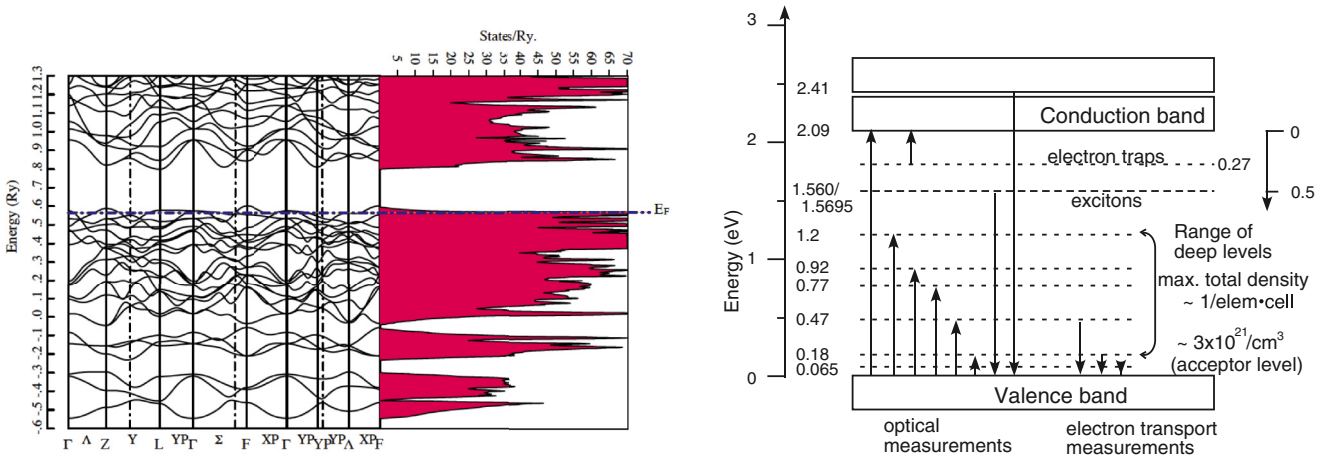

FIG. 2. (Color online) LDA band and DOS structure of $B_{13}C_2$. The names of the Brillouin zone are given in Ref. [33]. The right-hand site of the figure shows an energy diagram of the gap states reported by Werheit [34].

Transport properties have produced a specific model for the transport mechanism. Some studies conclude that an increase in conductivity as the C content decreases indicates that the chain structure changes from CBC to CBB [43]. However, this conclusion resulted from assuming a specific transport mechanism. The transport properties are not sensitive to the C content between 13.3 and 20 at. % [64]. Many macroscopic observations such as hardness [5] and ultrasonic measurements [65] do not help in determining the chain structure.

B. Theoretical studies

There are many theoretical studies of the defect structures of $B_{13}C_2$ [4,14,32,66]. To examine the stability of disordered states, such as $(B_{11}C)$(CBB), which were suggested by experimental data, the total energies of these structures have been examined by DFT. Bylander and Kleinman showed that the site exchange of a terminal C atom of the chain with an icosahedral B atom resulted in an increase in the total energy by 0.14 eV/atom or more [32]. Table I shows our calculations together with Bylander and Kleinman's results. Note that the energy of the perfect structure B_{12}(CBC) is lower by 0.86 eV/atom than the reference states of α-rhombohedral boron and diamond, and thus all the disordered structures listed in Table I are stable compared with their constituents. However, within $B_{13}C_2$, the energy increase of 0.14 eV/atom due to the disorders is so large that disordered states are virtually prohibited. Further calculations were performed to examine other defect states, which did not resolve the discrepancy [66–69].

Entropic effects have been suggested to resolve the discrepancy in the disordered states. Huhn and Widom proposed a statistical description of boron carbides in a compositional range of 13.3 to 20 at. % C [70,71]. However, the lower C content boundary of the structure was fixed as B_{12}(CBC), which may not be correct.

III. CONSTRUCTION OF MODEL

The evidence relating to the defect states suggests that there is a fundamental flaw in the structural models used in previous studies. A more appropriate model must be constructed.

Balakrishnarajan *et al.* provided a useful insight into the bonding nature of $B_{12}C_3$. Their results may share a common view with a model of the geometrical frustration proposed for β-rhombohedral boron [29]. Unfortunately, it is not easy to construct a new model for $B_{13}C_2$ using this model, because of the many defect configurations' with similar energies.

Instead, we analyzed the failures of previous models and used the following points as the basis for devising a better structural model for $B_{13}C_2$: (i) Both experimental and theoretical results indicate that $(B_{11}C)$ is energetically more favorable than B_{12}; and (ii) the CBC chain is the most desirable structure for the chain. Any attempt to modify this structure has failed to decrease the energy. Combining (ii) with (i) alone yields no new results. It merely shows that boron carbide of 20 at. % C is more stable than that of 13.3 at. % C. The formation energy of B_{12}(CBC), calculated as 0.015 (Bylander *et al.*) [13,32], 0.047 (Lazzari *et al.*) [14], and 0.040 eV/atom (this study), is lower than that of $(B_{11}C)$(CBC). Thus, the C content should be maintained at 13.3 at. % C. This requires the following third condition: (iii) the introduction of B-rich subunits to balance the extra C content.

This cannot be achieved by rearranging the constituent atoms within a primitive unit cell only. However, if the symmetry constraint is relaxed so that different unit cells can have different atomic arrangements while maintaining the long-range order of the Bravais lattice, a desirable chemical composition of $B_{13}C_2$ could be achieved.

A building block, B_4, was discovered in low C-content boron carbides (≈9 at. % C) by Yakel [72]. The B_4 unit may meet condition (iii). The population ratio of the CBC chains to B_4 units is approximately 3 to 1. From this observation, we can construct the prototype structural model (model I),

$$3 \times (B_{11}C)(CBC) + B_{12}(B_4) \qquad \text{(model I)},$$

which amounts to approximately $4 \times B_{13}C_2$. The difference is only one C atom in 61 atoms. Although introducing B_4 units may increase the total energy, the cost is paid by forming units of $(B_{11}C)$(CBC). However, this compensation results in breaking the periodicity of atomic arrangements in a unit cell. This way of creating disordered states is an unavoidable result of the compromise between the bonding and compositional

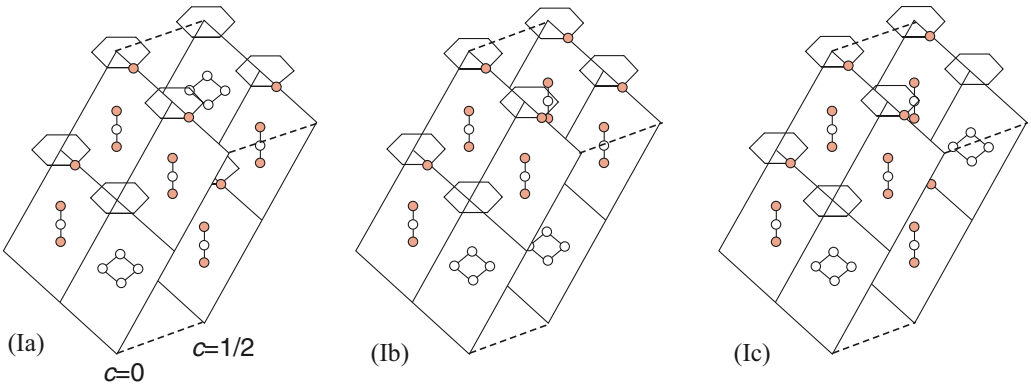

FIG. 3. (Color online) Configurations of structural model I. Red circles represent C atoms and hexagons represent icosahedra.

requirements. Thus, the situation is similar to the geometrical frustration found in β-rhombohedral boron [28,73]. Kwei and Morosin showed that B_4 units were observed at almost all C concentrations [55]. Therefore, it is not unreasonable to assume that B_4 units are present in high C concentrations.

In this work, the terms *nonstoichiometric state* and *disordered state* are used interchangeably. Although the global chemical composition is kept as $B_{13}C_2$, the disorder introduced by B_4 units results in local deviation from the stoichiometry within a primitive unit cell.

IV. RESULTS

For the total-energy calculations, a standard pseudopotential method was used. The OSAKA2K code was used [74]; the components of the code are LDA parameterized by Perdew and Zunger [75], the Perdew-Burke-Ernzerhof form of the generalized gradient approximation (GGA) [76], and Troullier-Martins pseudopotentials [77] with a fully separable Kleinman-Bylander form [78]. The LDA was used unless otherwise stated. We used a kinetic cutoff energy of 70 Ry and Γ-point sampling for supercell calculations. The convergence has been well tested in our previous studies [25]. Structural optimization was performed with a residual force of less than 10^{-3} Ry/bohr per atom and a residual stress of less than 10^{-4} Ry for the maximum component.

In this paper, we use the following conventions. Negative-energy differences with respect to the reference state indicate greater stability. The formation energy is a negative of the energy difference.

A. Fundamental model features

1. Total energy

We have constructed structural model I with $2 \times 2 \times 2$ supercells. Various atomic configurations were examined. Of these, three are shown in Fig. 3. For model I, the C content is 14.7 at. %, which is larger than the exact value of the composition of 13.3 at. % C. Because the reference state was the stoichiometric B_{12}(CBC) composition, a correction of one C atom is needed:

$$\Delta E = E_{\text{model I}} - \{4 \times E_{B_{12}(\text{CBC})} + E_{\text{C}}\}. \quad (1)$$

The reference state of C was diamond. The effect of this correction is small and eventually vanishes as the C content approaches the exact value of 13.3 at. % C. The results of the total energy are listed in Table II. For consistency, stoichiometric B_{12}(CBC) was also evaluated by a supercell of the same size. Introducing B_4 units to supercells breaks the crystal symmetry. However, the experimental structure has a high symmetry of $R\bar{3}m$. Therefore, the cell parameters were constrained to keep the sides of the cells the same length. Without this constraint, the total energy was slightly reduced, as shown in Table II. Because the reduction was slight, we ignored the effect of the cell constraints. By comparing the results in Table II with those in Table I, the energy increase caused by defects is reduced by more than half. Introducing B_4 units is an effective way to reduce the total energy, which could not be achieved by altering the chain and icosahedra alone.

Different positions of C at the p site of the icosahedron, $B_{11}C_{(p)}$, changed the total energy by less than 5 meV/atom. Therefore, the different arrangements of C positions in $B_{11}C_{(p)}$ were not taken into account.

2. Bonding behavior of B_4

The bonding behavior of the B_4 unit was examined with $B_{12}(B_4)$ and $(B_{11}C)(B_4)$ unit cells. Figure 4 shows the charge distribution of a $B_{12}(B_4)$ unit cell. The atom positions were fixed using the experimental values reported by Yakel [72]. The bonding in the B_4 unit is clearly covalent.

TABLE II. LDA energy difference and lattice-parameter difference of the $B_{13}C_2$ structural model I. Energy is given in eV/atom. The calculation error for the lattice parameters is estimated by taking experimental values reported by Kirfel *et al.* [16] as a reference. The relative errors in percent are shown. When no constraint is imposed on the lattice parameters, the average lattice-parameter value $\langle \Delta a_0 \rangle$ is used.

	Cell constraint		No constraint	
Type	ΔE	$\Delta a_0/a_0$	ΔE	$\langle \Delta a_0 \rangle / a_0$
B_{12}(CBC)	0	−1.24	0	−1.24
Ia	0.062	−1.87	0.062	−1.84
Ib	0.056	−1.54	0.051	−1.50
Ic	0.049	−1.63	0.045	−1.58

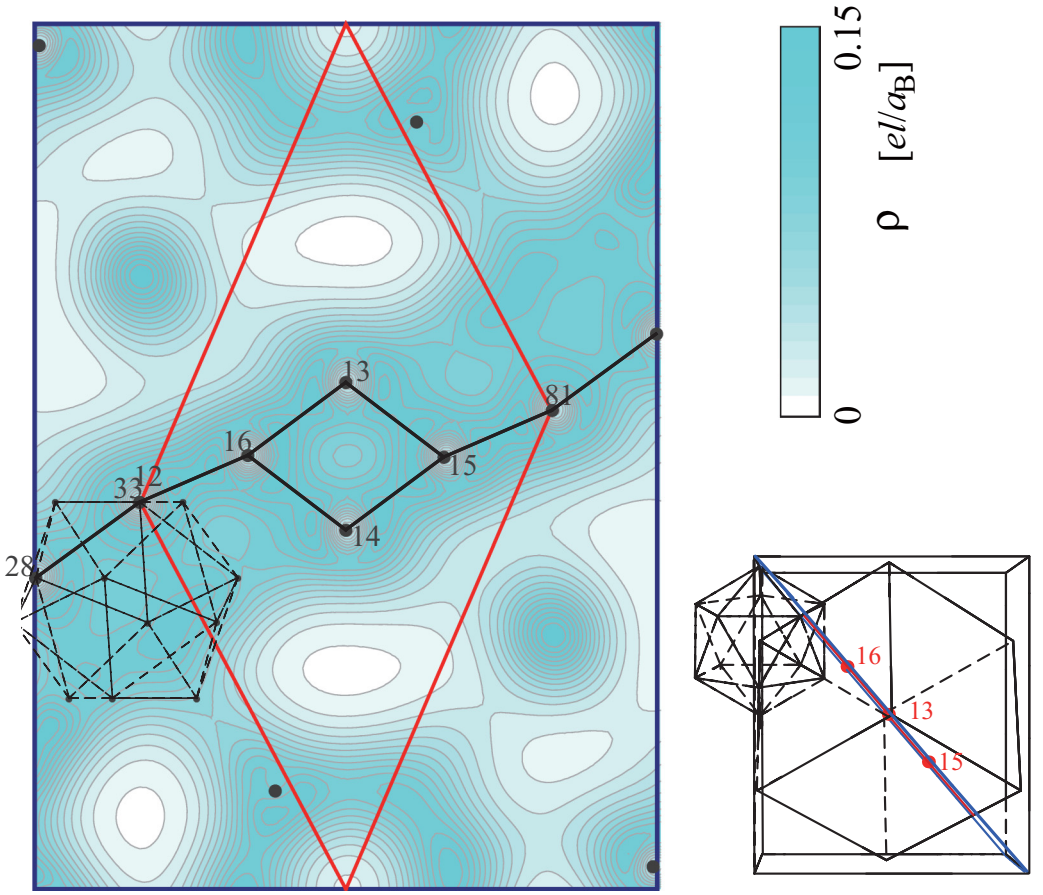

FIG. 4. (Color online) Charge density of $B_{12}(B_4)$. Red lines indicate the boundary of the primitive unit cell. The cut plane (blue) is shown in the right-hand figure, which is a top down view of the unit cell. The atoms are numbered.

Top atom 13 in the B_4 unit has three equivalent bonds, each connecting to an equatorial $B_{(e)}$ in the nearest icosahedra. The experimental bond length is 1.74 Å. Within a B_4 unit, atom 13 has two equivalent bonds, with a bond length of 1.72 Å, and a coordination number of 5. In contrast, side atom 16 has the shortest bond to a polar $B_{(p)}$ in the nearest icosahedron, with a bond length of 1.65 Å. As expected, this bond has the highest peak with a charge density of 0.28 el/a_B^3, which is not visible in Fig. 4. In addition, side atom 16 has two bonds within the B_4 unit and two weaker bonds with a bond length of 1.81 Å to $B_{(p)}$ in the nearest icosahedron. In either case, the B atoms have a coordination number of about 5, which is a common feature of icosahedron-based boron crystals.

According to Yakel [72], the four bonds of the B_4 unit should all be equal. However, after structural optimization, the B_4 became quite distorted. This can be understood by looking at Fig. 4. Atom 16 is pulled downwards, whereas atom 15 is pulled upwards. Consequently, one pair of B_4 bonds was elongated by 5.8%, whereas the other was elongated by 3.8%. We suppose that the regular rhombus B_4 is only an average, owing to the statistical distribution of the orientation of the B_4 surface around the c axis.

Another interesting feature of B_4 is that the B_4 plane is not on the vertical mirror symmetry planes, as shown in the right-hand side of Fig. 4. The experimental deflection angle, θ, of the B_4 plane from a vertical mirror symmetry plane is 19.5° [72]. The calculated values were substantially different from the experimental value, possibly for the same reason that explains the disagreement in the bond length of B_4. The deflection angle θ is sensitive to the location of the nearest-neighboring C atom.

B. Improvement

1. *Total energy*

Although the energy of the disordered structures was reduced compared with previous studies, we explored other low-energy structures. One-quarter of B_4 units in model I may be too large. Thus, a smaller number of B_4 units is appropriate.

Within supercells of $2 \times 2 \times 2$ size, this cannot be achieved simply by replacing $B_{12}(B_4)$ with $(B_{11}C)(CBC)$. Introducing a fraction of $B_{12}(CBC)$ resolved this and produced model II:

$$3 \times (B_{11}C)(CBC) + (B_{12})(B_4) + 4 \times (B_{12})(CBC) \qquad \text{(model II)}.$$

The C content was reduced to 14.0 at. %, which is closer to 13.3 at. %. Accordingly, the correction term for the C mismatch is reduced. We examined many atomic configurations for model II, some of which are shown in Fig. 5.

The energy differences of these structures compared with stoichiometric $B_{12}(CBC)$ show a clear improvement

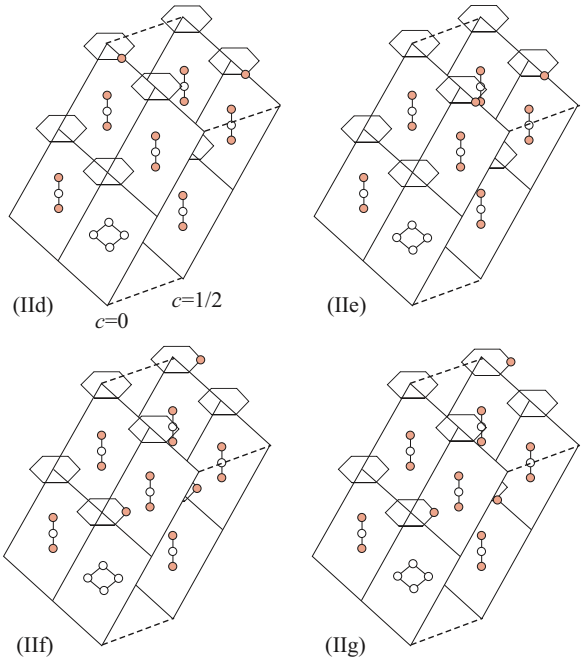

FIG. 5. (Color online) Structural model II. Red circles represent C atoms and hexagons represent icosahedra.

(Table III). The energy of all the disordered structures was almost the same as that of stoichiometric B_{12}(CBC); the energy difference was only several meV/atom, which is the limit of accuracy of the current DFT calculation for the formation energy [79]. There may be no unique structure to satisfy both the bonding requirement and the compositional requirement. This tradeoff produces many atomic configurations with energetically degenerate or almost degenerate states. Macroscopic numbers of degeneracy and nonuniqueness in structure are important features of frustrated systems. GGA improved agreement of the lattice parameters with the experimental value reported by Kirfel *et al.* [16], as shown in Table III.

Interestingly, our model can explain why the C content of boron carbides is limited to 20 at. %. When the C content is increased from 13.3 to 20 at. %, the B_4 units are successively replaced with CBC chains. After the B_4 units are completely removed, the highest C content structure (B_{11}C)(CBC) is achieved, which corresponds to a C content of 20 at. %.

TABLE III. LDA energy differences (in eV/atom) and lattice-parameter differences (relative unit of percent) for the $B_{13}C_2$ structural model. (*p*) indicates structures in which all icosahedral C atoms are located at the *p* site. (*e*) indicates structures in which at least one of the icosahedral C atoms is located at the *e* site.

		Cell constraint		
Type		ΔE	$\Delta a_0/a_0$	Notes
B_{12}(CBC)		0	−1.24	
(*p*)	IId	0.007	−1.27	
	IIe	0.011	−1.30	
(*e*)	IIf	0.004	−1.23	
	IIg	0.001	−1.19	
			−0.11	GGA calc.

In the 20-at. % compound, (B_{11}C)(CBC), an icosahedral C atom occupies a polar site. However, in a 13.3-at. % compound, this is not necessarily true. In the 20% C compound, occupation of an icosahedral C atom at the *p* site is only a way to avoid forming a direct C–C bond between a terminal C and an icosahedral C atom. We assume that boron carbides generally avoid forming direct C–C bonds. From this empirical rule, it follows that, in our model for $B_{13}C_2$, there is no reason for an icosahedral C atom to occupy the *e* site, when the *e*-site C atom is directly connected to a B_4 in a unit cell.

We list the results for the configurations of *e*-site C as models IIf and IIg in Table III. Placing the *e*-site C further reduced the total energy in many cases.

2. *Electronic structure*

The electronic structures of our models were calculated. Figure 6 shows an example of the DOS. The first gap state appeared 1.0 eV above the top of the valence band, and the second appeared 1.0 eV higher than the first one. The calculated DOS seemed to replicate the experimental gap states shown in Fig. 2. By constructing further large cells and adding different types of defects, many defect states can be created and may finally coalesce into a continuous band. There were two holes in the valence band, and thus the density of holes in a primitive unit cell (15 atom cell) was reduced to 0.25 hole/cell. This suggests that, as the cell size increases, the density of holes will vanish, resulting in an insulator.

It is difficult to attribute the experimentally observed gap states to specific types of defects, because of the many complex defect configurations. Calculation of the partial DOS nonetheless provides useful insights into the gap states. The right-hand side of Fig. 6 shows partial DOS for model IIg. Both of the two gap states have a large contribution from the B_4 units. This indicates that the B_4 bonds are weak; one pair of bonds was easily broken, as discussed in Sec. IVA2. In contrast, the contribution of C, whether it is a terminal $C_{(c)}$ or an icosahedral $C_{(e)}$, is small, meaning that the bonding requirement of C atoms is completely fulfilled.

3. *Phonon spectra*

We examined the phonon properties by calculating the Raman spectra. We performed frozen-phonon calculations, and the Raman intensity was calculated by the empirical bond-polarizability model [80,81]. There are many parameters for the polarizabilities associated with individual bonds. We did not attempt to find the best fit; rather we simply adapted the parameters which were used for calculating the anharmonic optical spectra of α-rhombohedral boron [82].

The calculated Raman spectra are compared with the experimental results reported by Tallant *et al.* [61] in Fig. 7. The figure shows that the theoretical and experimental results agree well. As the C content decreases, both the calculated and experimental frequencies decrease. This is expected, because of the strength of C bonding [86]. Also in this range, line broadening is observed experimentally, particularly the peaks at 490 and 520 cm^{-1}. These peaks correspond to the librational modes of the icosahedron [14]. The narrow linewidth of the librational modes has a special meaning for the anharmonic effect [83]. In our calculation, this anharmonic effect was

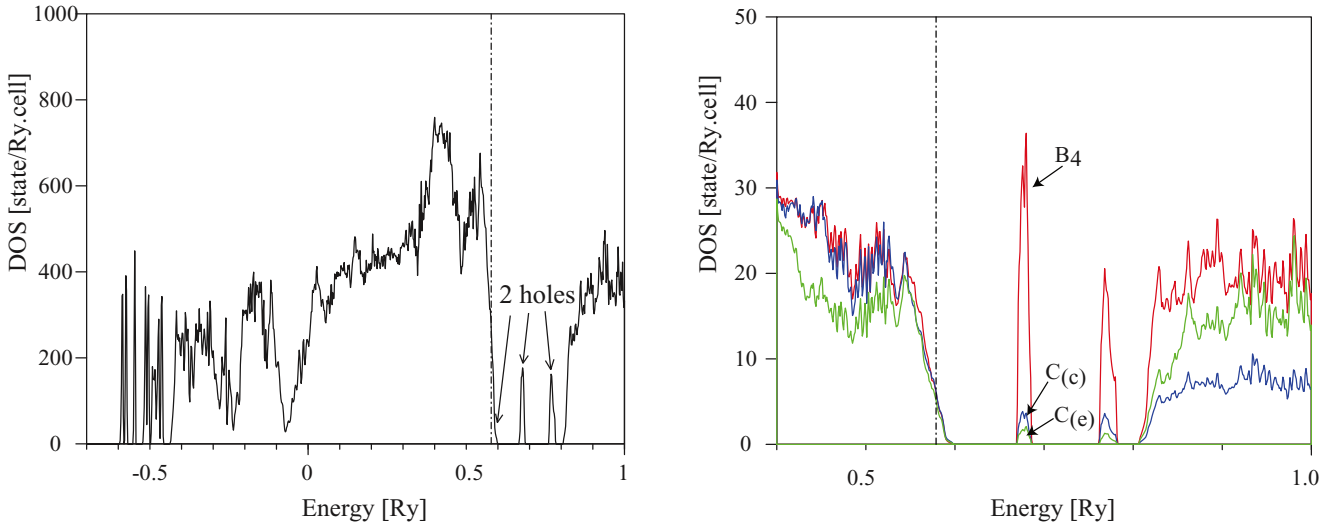

FIG. 6. (Color online) LDA DOS of model IIg. The left-hand figure shows the total DOS, whereas the right-hand figure shows the partial DOS split into its B_4, $C_{(e)}$, and $C_{(c)}$ components. The dashed line indicates the Fermi level.

not taken into account; the observed linewidths of individual modes are artifacts arising from the Gaussian broadening method. However, the broad features caused by band overlap are physically meaningful. The defect states in the supercells created many defect-induced modes and activated many modes that are otherwise silent. We discuss the significance of this broadening later.

In the calculation, weak peaks appeared on the low-frequency side. The 110-cm^{-1} mode was assigned to a twisting mode of the B_4 unit. The 355- and 403-cm^{-1} modes arose from the bending motion of the CBC chain, which were not Raman active in the high-symmetry structure. These modes together with the acoustic-branch modes may produce the low-frequency disorder-induced bands observed experimentally.

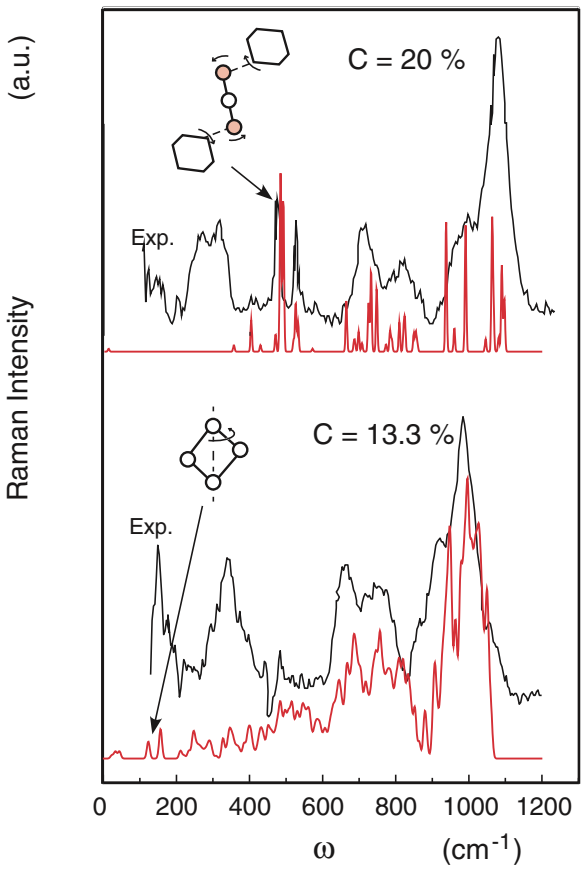

FIG. 7. (Color online) LDA Raman spectra (red lines) of boron carbides with compositions of 20 and 13.3 at. % C. Experimental spectra reported by Tallant *et al.* [61] are shown as black lines. Insets: Eigenvectors for some important normal modes.

V. DISCUSSION

A. Length of CBC chain

Experimentally, decreasing the C content from 20 to 13.3 at. % increases the cell size of $B_{1-x}C_x$ by about 1% [53,55], and similar values are obtained from the calculations. This is expected; because C atoms have a deep potential, the decrease in C content results in an increase of the lattice size. Calculations predict that the CBC chain lengthens by 2.7%, when stoichiometric B_{12}(CBC) was assumed. However, the opposite is observed experimentally, as discussed in Ref. [84]; the largest change is −2.4% obtained by neutron-scattering measurements [55], and virtually no change was observed in other experiments. Table III of Ref. [84] contains a summary of this data.

This discrepancy can be resolved by our model. The experimental value of the distance between B(13) and B(14) of B_4 (2.07 Å [72]) is shorter than that between the terminal C-C atoms in the chain (2.88 Å). If the effective C-C distance is defined as the average value between the C-C distance of the CBC chain and the B(13)-B(14) distance of B_4, the effective C-C distance of our model is 2.5% shorter than the C-C distance of the stoichiometric B_{12}(CBC). The C-C distance of high-symmetry B_{12}(CBC) is 2.7% longer than that of $B_{12}C_3$. This 2.7% increase is almost canceled out by the 2.5% reduction of the effective C-C distance caused by

the mixing of B_4. As a result, the length of the linear chain observed by x-ray diffraction does not expand with the cell.

Another possible reason for the shrinkage of the chain as the cell size increases is the presence of vacancies at the central site of the chain. Kwei and Morosin reported a large concentration of vacancies at this site and casted a question whether this concentration of vacancies all comes from B_4 units [55]. Their study, though highly accurate, did not answer the question definitively because many of the parameters were assumed. We propose that the majority of vacancies at the central site is produced by replacing the CBC chain with B_4 units, because creating a vacancy requires a large amount of energy.

B. Stiffness of the linear chain

In relation to the softening-enhanced thermoelectric power [85], Emin and coworkers argued that the chain of boron carbide is soft [48,49]. This argument is based on the assignment of the low-frequency bands at 490 and 520 cm^{-1} to the stretching vibrations of the chain. As described in Sec. IIA2, they interpreted the broadening of the 490- and 520-cm^{-1} bands as evidence for more disordered states in the chain. As the C content decreases from 20 to 13.3 at. %, first a terminal C in the chain is replaced with B, and then an icosahedral C is replaced [48,61].

Our calculations show that, even when the structure of the CBC chain was maintained, the linewidth of the 490- and 520-cm^{-1} bands was broadened. Hence, the broadening of these bands probably occurs because of the introduction of B_4 units. The terminal C atoms do participate in these modes, although not through their stretching modes (Fig. 7). The chain rotates around an axis in the *ab* plane, thus the bond lengths of the chain do not change. The frequency is mainly determined by the rotational displacement of the icosahedra. The stretching modes of the chain appear around 1000 cm^{-1} for the symmetric and at 1560 cm^{-1} for the antisymmetric mode [86], and the chain must be stiff.

An increase in the thermal factors in the x-ray analysis was interpreted as more evidence for a soft chain by Emin and coworkers [12,53,54]. However, the involvement of B_4 can explain the increase in the thermal factor of the chain atoms. First, introducing B_4 increases the thermal factor of the central chain atom, because B_4 does not have a central atom. Second, B_4 also affects the thermal factor of the terminal C atoms in the *c* direction, because the shorter B-B distance of B_4 is combined with the C-C distance of the chain.

Last, we note that, despite its stiffness, the chain also possesses soft properties. Our phonon calculations showed that the bending mode of the chain has a low frequency of 355 cm^{-1}. The central B atom of the chain can be easily displaced from the chain axis [87], so a large displacement would be expected.

VI. CONCLUSION

We have demonstrated that introducing 10% B_4 units profoundly changes the model of $B_{13}C_2$. Many problems with $B_{13}C_2$, such as the metal/insulator behavior, band gap, and defect states, were solved. The broadening of Raman peaks, the chain length, and the abnormal thermal factor of x-ray diffraction can be explained by the presence of B_4 units. Despite the appearance of the stoichiometry of $B_{13}C_2$ and its high symmetry, a strong driving force acts on formation of defect states. One electron deficiency of a unit cell B_{12}(CBC) is locally recovered by replacement with another structural unit, (B_{11}C)(CBC). This method of fulfilling the bonding requirement produces deviation from the chemical composition. However, introducing B_4 units retains the global chemical composition. The number of ways to arrange different cell structures while maintaining the chemical composition is large, and many are almost degenerate, which appears to result in geometrical frustration.

Although we have examined $B_{13}C_2$ in this paper, the method can be extended to a wide range of boron, boron-rich crystals, and other hard semiconductors that are predicted to be metals. Crystalline BC_5, the structure of which is under debate [88], may be such an example.

ACKNOWLEDGMENTS

This work is supported by the Grant-in-Aid for Scientific Research on Innovative Areas “Materials Design through Computics: Complex Correlation and Non-Equilibrium Dynamics” (Grant No. 22104011) from the Ministry of Education, Culture, Sports, Science, and Technology, Japan.

[1] D. Emin, Phys. Today **40**, 55 (1987).
[2] F. Thévenot, J. Euro. Ceramic Soc. **6**, 205 (1990).
[3] H. Werheit, J. Phys.: Conf. Ser. **176**, 012019 (2009).
[4] N. Vast, J. Sjakste, and E. Betranhandy, J. Phys.: Conf. Ser. **176**, 012002 (2009).
[5] V. Domnich, S. Reynaud, R. A. Haber, and M. Chhowalla, J. Am. Ceramic Soc. **94**, 3605 (2011).
[6] D. Gosset and M. Colin, J. Nucl. Mater. **183**, 161 (1991).
[7] H. Werheit, A. Leithe-Jasper, T. Tanaka, H. W. Rotter, and K. A. Schwetz, J. Solid State Chem. **177**, 575 (2004).
[8] H. K. Clark and J. L. Hoard, J. Am. Chem. Soc. **65**, 2115 (1943).
[9] J. H. Hoard and R. E. Hughes, *The Chemistry of Boron and Its Compounds*, edited by E. L. Mueterties (Wiley, New York, 1965).
[10] A. C. Larson and D. T. Cromer, Acta Crystallogr. A **28**, S53 (1972), abstract IV-01.
[11] A. C. Larson, in *Boron-Rich Solids*, edited by D. Emin, T. Aselage, C. L. Beckel, I. A. Howard, and C. Wood, AIP Conf. Proc. No. 140 (AIP, New York, 1986), p. 109.
[12] B. Morosin, A. W. Mullendore, D. Emin, and G. Slack, in *Boron-Rich Solids*, edited by D. Emin, T. Aselage, C. L. Beckel, I. A. Howard, and C. Wood, AIP Conf. Proc. No. 140 (AIP, New York, 1986), p. 70.
[13] D. M. Bylander, L. Kleinman, and S. Lee, Phys. Rev. B **42**, 1394 (1990).
[14] R. Lazzari, N. Vast, J. M. Besson, S. Baroni, and A. Dal Corso, Phys. Rev. Lett. **83**, 3230 (1999); **85** 4194(E) (2000).

[15] F. Mauri, N. Vast, and C. J. Pickard, Phys. Rev. Lett. **87**, 085506 (2001).
[16] A. Kirfel, A. Gupta, and G. Will, Acta Crystallogr. B **35**, 1052 (1979).
[17] A. Kirfel, A. Gupta, and G. Will, Acta Crystallogr. B **35**, 2291 (1979).
[18] A. Kirfel, A. Gupta, and G. Will, Acta Crystallogr. B **36**, 1311 (1980).
[19] D. R. Armstrong, J. Balland, P. G. Pukins, G. Will, and A. Kirfel, Acta Crystallogr. B **39**, 324 (1983).
[20] M. Calandra, N. Vast, and F. Mauri, Phys. Rev. B **69**, 224505 (2004).
[21] H. Werheit and U. Kuhlmann, J. Phys.: Condens. Matter **23**, 435501 (2011).
[22] R. Franz and H. Werheit, Europhys. Lett. **9**, 145 (1989).
[23] K. Kimura, M. Takeda, M. Fujimori, R. Tamura, H. Matsuda, R. Schmechel, and H. Werheit, J. Solid State Chem. **133**, 302 (1997).
[24] R. Schmechel and H. Werheit, J. Phys.: Condens. Matter **11**, 6803 (1999).
[25] A. Masago, K. Shirai, and H. Katayama-Yoshida, Phys. Rev. B **73**, 104102 (2006).
[26] M. J. van Setten, M. A. Uijttewaal, G. A. de Wijs, and A. de Groot, J. Am. Chem. Soc. **129**, 2458 (2007).
[27] M. Widom and M. Mihalkovič, Phys. Rev. B **77**, 064113 (2008).
[28] T. Ogitsu, F. Gygi, J. Reed, Y. Motome, E. Schwegler, and G. Galli, J. Am. Chem. Soc. **131**, 1903 (2009).
[29] M. M. Balakrishnarajan, P. D. Pancharatna, and R. Hoffmann, New J. Chem. **31**, 473 (2007).
[30] T. Ogitsu, F. Gygi, J. Reed, M. Udagawa, Y. Motome, E. Schwegler, and G. Galli, Phys. Rev. B **81**, 020102(R) (2010).
[31] K. Shirai and N. Uemura, Solid State Sci. **14**, 1609 (2012).
[32] D. M. Bylander and L. Kleinman, Phys. Rev. B **43**, 1487 (1991).
[33] K. Shirai, H. Dekura, and A. Yanase, J. Phys. Soc. Jpn. **78**, 084714 (2009).
[34] H. Werheit, J. Phys.: Condens. Matter **18**, 10655 (2006).
[35] H. Werheit, H. Binnenbruck, and A. Hausen, Phys. Status Solidi B **47**, 153 (1971).
[36] H. Werheit, V. Filipov, U. Schwarz, M. Armbrüster, A. Leithe-Jasper, T. Tanaka, and S. O. Shalamberidze, J. Phys.: Condens. Matter **22**, 045401 (2010).
[37] H. Werheit, H. W. Rotter, S. O. Shalamberidze, A. Leithe-Jasper, and T. Tanaka, Phys. Status Solidi B **248**, 1275 (2011).
[38] D. B. Bullett, J. Phys. C **15**, 415 (1982).
[39] H. Werheit and K. de Groot, Phys. Status Solidi B **97**, 229 (1980).
[40] C. Wood and D. Emin, Phys. Rev. B **29**, 4582 (1984).
[41] M. Bouchacourt and F. Thévenot, J. Mater. Sci. **20**, 1237 (1985).
[42] H. Werheit, U. Kuhlmann, R. Franz, W. Winkelbauer, B. Herstell, and D. R. Neisius, in *Boron-Rich Solids*, AIP Conf. Proc. No. 231 (AIP, New York, 1991), p. 104.
[43] G. A. Samara, H. L. Tardy, E. L. Venturini, T. L. Aselage, and D. Emin, Phys. Rev. B **48**, 1468 (1993).
[44] L. J. Azevedo, E. L. Venturini, D. Emin, and C. Wood, Phys. Rev. B **32**, 7970 (1985).
[45] D. Emin, in *Boron-Rich Solids*, edited by D. Emin, T. Aselage, C. L. Beckel, I. A. Howard, and C. Wood, AIP Conf. Proc. No. 140 (AIP, New York, 1986), p. 189.
[46] I. A. Howard, C. L. Beckel, and D. Emin, Phys. Rev. B **35**, 9265 (1987).
[47] D. Emin, Phys. Rev. B **38**, 6041 (1988).
[48] T. L. Aselage, D. R. Tallant, and D. Emin, Phys. Rev. B **56**, 3122 (1997).
[49] T. L. Aselage, D. Emin, and S. S. McCready, Phys. Rev. B **64**, 054302 (2001).
[50] H. Werheit, H. W. Rotter, F. D. Meyer, H. Hillebrecht, S. O. Shalamberidze, T. G. Abzianidze, and E. G. Esadze, J. Solid State Chem. **177**, 569 (2004).
[51] H. Werheit, U. Kuhlmann, H. W. Rotter, and S. O. Shalamberidze, J. Phys.: Condens. Matter **22**, 395401 (2010).
[52] H. Kim and M. Kaviany, Phys. Rev. B **87**, 155133 (2013).
[53] T. L. Aselage and D. Emin, in *Boron-Rich Solids*, AIP Conf. Proc. No. 231 (AIP, New York, 1991), p. 177.
[54] B. Morosin, T. L. Aselage, and D. Emin, in *Boron-Rich Solids*, AIP Conf. Proc. No. 231 (AIP, New York, 1991), p. 193.
[55] G. H. Kwei and B. Morosin, J. Phys. Chem. **100**, 8031 (1996).
[56] A. H. Silver and P. H. Bray, J. Chem. Phys. **31**, 247 (1959).
[57] T. M. Duncan, J. Am. Chem. Soc. **106**, 2270 (1984).
[58] P. J. Bray, in *Boron-Rich Solids*, edited by D. Emin, T. Aselage, C. L. Beckel, I. A. Howard, and C. Wood, AIP Conf. Proc. No. 140 (AIP, New York, 1986), p. 142.
[59] R. J. Kirkpatrick, T. Aselage, B. L. Phillips, and B. Montez, in *Boron-Rich Solids*, AIP Conf. Proc. No. 231 (AIP, New York, 1991), p. 261.
[60] J. A. Shelnutt, B. Morosin, D. Emin, A. Mulledore, G. A. Slack, and C. Wood, in *Boron-Rich Solids*, edited by D. Emin, T. Aselage, C. L. Beckel, I. A. Howard, and C. Wood, AIP Conf. Proc. No. 140 (AIP, New York, 1986), p. 312.
[61] D. R. Tallant, T. L. Aselage, A. N. Campbell, and D. Emin, Phys. Rev. B **40**, 5649 (1989).
[62] H. Werheit, T. Au, R. Shmechel, S. O. Shalamberidze, G. I. Kalandadze, and A. M. Eristavi, J. Solid State Chem. **154**, 79 (2000).
[63] H. Werheit, R. Shmechel, U. Kuhlmann, T. U. Kampen, W. Mönch, and A. Rau, J. Alloys and Compounds **291**, 28 (1999).
[64] G. A. Samara, D. Emin, and C. Wood, Phys. Rev. B **32**, 2315 (1985).
[65] J. H. Gieske, T. L. Aselage, and D. Emin, in *Boron-Rich Solids*, AIP Conf. Proc. No. 231 (AIP, New York, 1991), p. 376.
[66] J. E. Saal, S. Shang, and Z.-K. Liu, Appl. Phys. Lett. **91**, 231915 (2007).
[67] S. Aydin and M. Simsek, Phys. Status Solidi B **246**, 62 (2009).
[68] R. Raucoules, N. Vast, E. Betranhandy, and J. Sjakste, Phys. Rev. B **84**, 014112 (2011).
[69] E. Betranhandy, N. Vast, and J. Sjakste, Solid State Sci. **14**, 1683 (2012).
[70] W. P. Huhn and M. Widom, J. Stat. Phys. **150**, 432 (2013).
[71] M. Widom and W. P. Huhn, Solid State Sci. **14**, 1648 (2012).
[72] H. L. Yakel, Acta Crystallogr. B **31**, 1797 (1975).
[73] T. Ogitsu, E. Schwegler, and G. Galli, Chem. Rev. **113**, 3425 (2013).
[74] http://www.cmp.sanken.osaka-u.ac.jp/~koun/osaka.html.
[75] J. P. Perdew and A. Zunger, Phys. Rev. B **23**, 5048 (1981).
[76] J. P. Perdew, K. Burke, and M. Ernzerhof, Phys. Rev. Lett. **77**, 3865 (1996).
[77] N. Troullier and J. L. Martins, Phys. Rev. B **43**, 1993 (1991).
[78] L. Kleinman and D. M. Bylander, Phys. Rev. Lett. **48**, 1425 (1982).
[79] K. Shirai, H. Fujita, and H. Katayama-Yoshida, Phys. Status Solidi B **235**, 526 (2003), and references therein.

[80] A. A. Maradudin and E. Burstein, Phys. Rev. **164**, 1081 (1967).
[81] S. Go, H. Bilz, and M. Cardona, Phys. Rev. Lett. **34**, 580 (1975).
[82] K. Shirai and H. Katayama-Yoshida, Physica B **263–264**, 791 (1999).
[83] K. Shirai and H. Katayama-Yoshida, J. Phys. Soc. Jpn. **67**, 3801 (1998).
[84] K. Shirai and H. Katayama-Yoshida, J. Solid State Chem. **154**, 20 (2000).
[85] D. Emin, Phys. Rev. B **59**, 6205 (1999).
[86] K. Shirai and S. Emura, J. Phys.: Condens. Matter **8**, 10919 (1996).
[87] K. Shirai and H. Katayama-Yoshida, in *Proceedings of the 25th International Conference on the Physics of Semiconductors* (Springer, Osaka, 2000), pp. 1673–1674.
[88] V. L. Solozhenko, O. O. Kurakevych, D. Andrault, Y. Le Godec, and M. Mezouar, Phys. Rev. Lett. **102**, 015506 (2009); **102** 179901(E) (2009).